2014 International Conference on Unmanned Aircraft Systems (ICUAS)
May 27-30, 2014. Orlando, FL, USA

Dynamic Modeling of a Fixed-Wing VTOL UAV

Aslihan Vuruskan[1], Burak Yuksek[2], Ugur Ozdemir[3], Adil Yukselen[4] Gokhan Inalhan[5]

***Abstract* — This paper presents a transition-flight mathematical model of a civil tilt-rotor VTOL unmanned aerial vehicle (UAV) TURAC. Forces and moments acting on the UAV body are calculated using Newton's second law. Aerodynamic effects of free airstream and propeller airstream are defined separately. CFD analyses are performed to specify aerodynamic coefficients for transitional flight regime. The trim point is mathematically defined with respect to angle of attack, tilt angle, airspeed, thrust of tilt-rotor and coaxial fan are defined during transitional flight. A transitional flight scenario is developed with force and moment equations.**

I. INTRODUCTION

In recent years, civil UAVs have been used widely in areas such as agricultural observation, wildlife protection, and traffic monitoring. Various types of UAVs such as quadrotor, tilt-rotor/tilt-wing and vertical take-off and landing UAV, etc. are designed for different operational aims. Each of these airframe concepts has advantages and disadvantages depending on the design specifications.

Unmanned rotorcrafts are able to takeoff and land vertically on both flat and rugged surfaces and do not need a helipad, because of their low weight and small dimensions. Observation or reconnaissance missions of a specified area can be performed for several minutes while hovering, which is the most important capability of the unmanned rotorcrafts.

Despite the advantages of the hover flight regime, unmanned rotorcrafts cannot be used for operations which require high speed, altitude, payload capacity, or long flight range. Compared to rotorcrafts, fixed wing UAVs have remarkable payload capacity for different types of operations and aims. Additionally, mini and micro fixed-wing UAVs may be hand or catapult launched, which is a vital capability in rural areas. Medium and high altitude UAVs need a runway for takeoff and landing because of their weight and dimensions.

* Research is supported in part by the Republic of Turkey, Ministry of Science, Industry and Technology SANTEZ Program Contract 1585.STZ.2012-2 and HAVELSAN A.S.

[1] A.V. is M.Sc. student at the Istanbul Technical University, 34469, Istanbul, Turkey. (Corresponding Author e-mail: vuruskan@itu.edu.tr)
[2] B. Y. is a Ph.D. student at the Istanbul Technical University
[3] U. O. is a Ph.D. candidate at the Istanbul Technical University
[4] A. Y. is Professor at the Istanbul Technical University
[5] G. I. is Associate Professor at the Istanbul Technical University, Faculty of Aeronautics and Astronautics, 34469, Istanbul, Turkey (e-mail: inalhan@itu.edu.tr) and G. I. is the PI of the associated Research Project.

Especially in military applications, it is important to be able to operate UAVs in different conditions. For this reason, recent studies have focused on vertical takeoff and landing UAVs, which combine the advantages of both rotorcrafts and fixed-wing UAVs. Panther (Israel Aerospace Industries), Eagle Eye (Bell Helicopter), and AD-150 (American Dynamics Flight System) are example systems for VTOL UAVs designed for military operations.

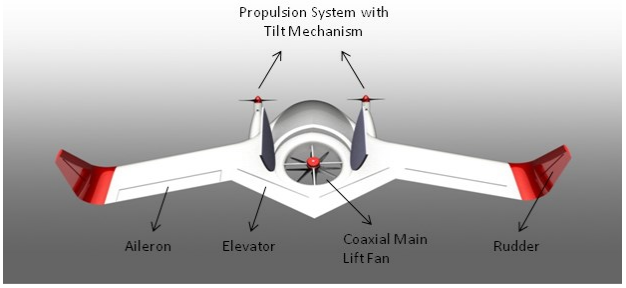

(a)

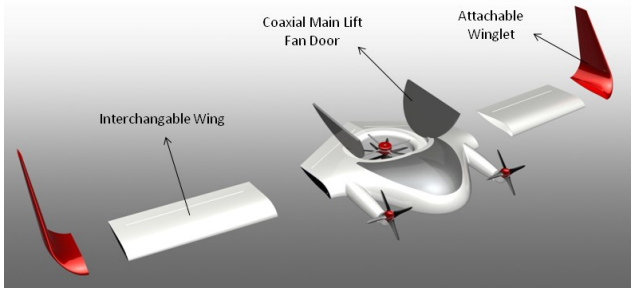

(b)

Figure 1. a) Control surfaces and propulsion system. b) Expanded view of structural elements.

After evaluating the above-mentioned advantages and disadvantages of the different types of UAVs, a TURAC civil tilt-rotor VTOL UAV is presented, designed and prototyped by the Control and Avionics Laboratory of the Istanbul Technical University [1].

Control surfaces and structural elements of the TURAC are shown in Fig. 1a and Fig. 1b. General specifications are given in Table 1.

Table 1. TURAC specifications

Wingspan	4.2 m
Length	1.8 m
Height	1.05 m
Front Propeller Diameter	0.43 m

Empty Weight	39 kg
Maximum Takeoff Weight	47 kg
Cruise Speed	20 m/s
Mission Altitude	1000 m

TURAC, which has a blended wing concept, is able to takeoff vertically from flat or rugged ground and perform hover flight, like an unmanned rotorcraft with two tilt rotors and main coaxial lifting fan. Seventy percent of the total thrust is provided by the coaxial rotor while hovering. In the transitional flight regime, tilting mechanisms are rotated simultaneously to generate horizontal thrust force, and acceleration is created by the horizontal projection of the propulsion. When the UAV exceeds the stall speed, the rotations of the tilt rotors are completed and the UAV enters the horizontal flight regime, like a conventional aircraft.

Figure 2. The TURAC hovering during a flight test.

During takeoff and landing, the main coaxial fan is open. In forward flight, it is closed by the doors. The propulsion system includes brushless direct-current motors and Lithium Polymer batteries which provide high performance. The wings and winglets are detachable, an advantage for easy transportation and changing of the wingspan, according to mission requirements.

In the literature, several experimental, numerical and analytical studies have been performed to define mathematical models and aerodynamic features of tilt-rotor aircrafts during flight regimes. In one of the studies on simulation and control, dynamic modeling, control, and design optimization of micro VTOL UAVs focused on the hover regime [2]. Another study includes linear and nonlinear control techniques, which are based on Lyapunov theory, Proportional Integral Derivative (PID) and Linear Quadratic (LQ), backstepping, and sliding-mode control algorithms for VTOLs [3].

In the transitional flight regime, dynamic models of the airframe include both hover and forward flight dynamics. Generally, studies on dynamic models of the transition regime also include the other two regimes. One of these studies describes motion equations of the tilt-rotor UAV in three flight regimes. The motion equations, which are linearized at trim flight conditions, are used for a stability analysis of the UAV [4]. Dynamic models of the UAV are represented with Newtonian equations for hover and forward flight [5]. The forces and moments acting on the UAV body are defined schematically. The longitudinal dynamic modeling of quad-tilting rotor is defined by kinematic transformations. Aerodynamic forces in three regimes and the strategy for a control algorithm is defined at the end of the study [6].

Today, aerodynamic analysis of tilt-rotor UAVs is an interesting and popular research area. Most studies are can be divided up as aerodynamic analyses of hover, transition, and forward flight regimes. They use analytical, experimental, and numerical methods, which include different kind of computation algorithms and software. Computational Fluid Dynamics (CFD) is one of the commonly used methods to determine the flowfield around tilt-rotor UAV airframes and to define the aerodynamic coefficients in different flight regimes.

In the hover regime, research has been done experimentally and numerically, such as the CFD method to define rotor/wing interaction. In one of the studies, a quad tiltrotor in hover mode is modeled and analyzed by using the CFD method. The pressure distribution on the wing, flowfield around the vehicle, and spanwise loading is investigated in and out of ground effect [7]. Another study that includes CFD analyses of full and half-span V-22 tilt-rotor configuration in hover mode has been done to observe flowfield around the vehicle. Rotor performance differences between two different models are evaluated [8]. Also, there are some experimental studies in the literature. One of them is with a quarter-scale V-22 tilt-rotor aircraft in hover mode. The topics of the study are rotor/wing interaction, aircraft aerodynamics, pressure distribution, and force loading along wingspan [9].

Studies about aerodynamic analysis of aircraft are mostly about hover and forward flight regime. However, transitional flight is the most complex case due to flowfield around UAV, rotor/wing interaction, pressure, and force loading through wingspan. In the literature, there is no research on flowfield around aircraft in transition mode using CFD or other numerical methods. In some experiments, research has been done with different flap deflections to develop rotor/wing interactions, pressure, force loading, and velocity distribution along wingspan [10, 11].

Research on forward flight regimes of tiltrotors or conventional aircrafts with the CFD method are very common in the literature. Performance and design of conventional tiltrotors and quad tiltrotors are investigated using the forward flight regime. Lift-to-drag ratio for both concepts is based on interference, reduction in rotor tip speed, and the change on rotor rotational direction [12]. The UAVs are tested and analyzed using wind tunnels and CFD methods to define flowfield around the airframe and aerodynamic coefficients [13, 14]. Propeller/wing interaction on multi-engined transport aircraft is investigated by modeling the propeller as an actuator disk, as in the CFD method [15]. Furthermore, aerodynamic stability and control coefficients of TR-E2S1 tilt-rotor aircraft are calculated with the CFD

method and the wind tunnel tests. The results from both methods are evaluated and compared at the end of the study [16]. The same methods are applied to V-22 Osprey tilt-rotor aircraft in forward flight regime [17]. In [18], Yak-54 is analyzed aerodynamically and results are compared from Vorstab, Fluent, and Aircraft Advanced Analysis (AAA).

II. MATHEMATICAL MODELING

A. General Equations of Motion

The general equations of motion for the UAV are obtained based on Newton's second law. According to the law of motion, summing all external forces acting on a body is equal to the time derivative of its momentum with respect to inertial space, as presented mathematically in (1) [19].

$$\sum \mathrm{F} = \frac{\mathrm{d}}{\mathrm{dt}}(\mathrm{mV}) \tag{1}$$

where F, m, V are force, mass and total speed.

The total moment on a body is defined as the time derivative of its moment of momentum (angular momentum) with respect to the inertial space according to Newton's second law of motion. The mathematical expression of the total moment is shown in (2) [19].

$$\sum \mathrm{M} = \frac{\mathrm{dH}}{\mathrm{dt}} \tag{2}$$

where M and H are moment and angular momentum.

Before the derivation step, it is necessary to make following assumptions [20]:

- The XZ plane of the UAV body axis system is the symmetry plane.
- The mass of the UAV remains constant.
- The UAV is a rigid body.
- The earth is the inertial reference.

Body and Earth axis systems are defined as shown in Fig. 3.

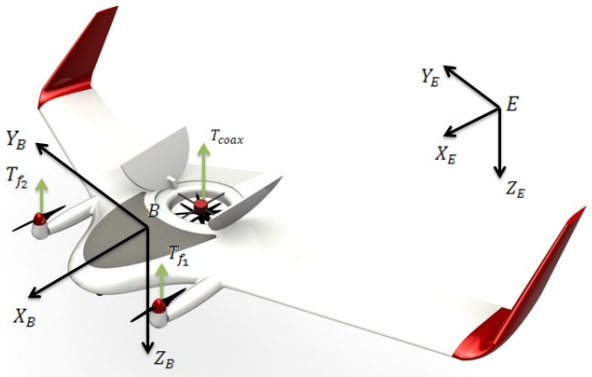

Figure 3. Earth and body axis systems.

Using Newton's second law of motion and the above-mentioned assumptions, force and moment equations are obtained, as shown in (3) and (4). External forces consist of gravity, aerodynamic, and thrust forces. Similarly, external moments consist of aerodynamic and thrust moments [21].

$$\begin{aligned} \mathrm{m}(\dot{\mathrm{U}} + \mathrm{QW} - \mathrm{RV}) &= \mathrm{F_{G_x}} + \mathrm{F_{A_x}} + \mathrm{F_{T_x}} \\ \mathrm{m}(\dot{\mathrm{V}} + \mathrm{RU} - \mathrm{PW}) &= \mathrm{F_{G_y}} + \mathrm{F_{A_y}} + \mathrm{F_{T_y}} \\ \mathrm{m}(\dot{\mathrm{W}} + \mathrm{PV} - \mathrm{QU}) &= \mathrm{F_{G_z}} + \mathrm{F_{A_z}} + \mathrm{F_{T_z}} \end{aligned} \tag{3}$$

$$\begin{aligned} \dot{\mathrm{P}}\mathrm{I_{xx}} + \mathrm{QR}(\mathrm{I_{zz}} - \mathrm{I_{yy}}) - (\dot{\mathrm{R}} + \mathrm{PQ})\mathrm{I_{xz}} &= \mathrm{L_A} + \mathrm{L_T} \\ \dot{\mathrm{Q}}\mathrm{I_{yy}} - \mathrm{PR}(\mathrm{I_{zz}} - \mathrm{I_{xx}}) + (\mathrm{P^2} - \mathrm{R^2})\mathrm{I_{xz}} &= \mathrm{M_A} + \mathrm{M_T} \\ \dot{\mathrm{R}}\mathrm{I_{zz}} + \mathrm{PQ}(\mathrm{I_{yy}} - \mathrm{I_{xx}}) + (\mathrm{QR} - \dot{\mathrm{P}})\mathrm{I_{xz}} &= \mathrm{N_A} + \mathrm{N_T} \end{aligned} \tag{4}$$

where U, V, W, P, Q, and R are linear and angular velocities of the UAV body. Gravitational, aerodynamic and thrust effects are defined using G, A, and T indices. F, L, M, and N denote force, roll moment, pitch moment, and yaw moment, respectively. Inertia moments are denoted using $\mathrm{I_{xx}}, \mathrm{I_{yy}}, \mathrm{I_{zz}}, \mathrm{I_{xz}}$.

The angular velocities of the UAV are transformed from the Earth axis system to the aircraft body axis system using transformation matrix R, as given in (5). Body angular velocities are obtained using the R matrix, as shown in (6).

$$\mathrm{R} = \begin{bmatrix} 1 & 0 & -\sin\theta \\ 0 & \cos\phi & \sin\phi\cos\theta \\ 0 & -\sin\phi & \cos\phi\cos\theta \end{bmatrix} \tag{5}$$

$$\begin{bmatrix} \mathrm{P} \\ \mathrm{Q} \\ \mathrm{R} \end{bmatrix} = \mathrm{R} \begin{bmatrix} \dot{\phi} \\ \dot{\theta} \\ \dot{\psi} \end{bmatrix} \tag{6}$$

where ϕ, θ, ψ are Euler angles.

The coordinates of the flight path with respect to Earth axis system are obtained using (7) as shown below [21].

$$\begin{aligned} \dot{\mathrm{x}}_\mathrm{E} &= \mathrm{U}\mathrm{c}\theta\,\mathrm{c}\,\psi + \mathrm{V}(\mathrm{s}\,\phi\,\mathrm{s}\,\theta\,\mathrm{c}\,\psi - \mathrm{c}\,\phi\,\mathrm{s}\,\psi) \\ &\quad + \mathrm{W}(\mathrm{c}\,\phi\,\mathrm{s}\,\theta\,\mathrm{c}\,\psi + \mathrm{s}\,\phi\,\mathrm{s}\,\psi) \\ \dot{\mathrm{y}}_\mathrm{E} &= \mathrm{U}\,\mathrm{c}\,\theta\,\mathrm{s}\,\psi + \mathrm{V}(\mathrm{s}\,\phi\,\mathrm{s}\,\theta\,\mathrm{s}\,\psi + \mathrm{c}\,\phi\,\mathrm{c}\,\psi) \\ &\quad + \mathrm{W}(\mathrm{c}\,\phi\,\mathrm{s}\,\theta\,\mathrm{s}\,\psi - \mathrm{s}\,\phi\,\mathrm{s}\,\psi) \\ \dot{\mathrm{z}}_\mathrm{E} &= -\mathrm{U}\,\mathrm{s}\,\theta + \mathrm{V}\,\mathrm{s}\,\phi\,\mathrm{c}\,\theta + \mathrm{W}\,\mathrm{c}\,\phi\,\mathrm{c}\,\theta \end{aligned} \tag{7}$$

B. Modeling of Transition Flight

Transitional flight is a complex regime between hover and horizontal flight. Forces and moments acting on the UAV body change continuously due to the tilting of the front propellers. Before deriving the dynamic equations of transitional flight, it is useful to define some geometrical dimensions and thrust forces.

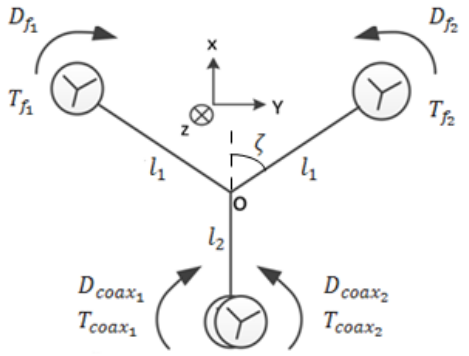

Figure 4: Force, moment, and some geometrical dimensions of the UAV.

In Fig. (4), T_{f_1} and T_{f_2} are thrusts of the tilt propellers, D_{f_1} and D_{f_2} are drag moments of the tilt propellers, T_{coax_1} and T_{coax_2} are thrusts of the coaxial fan propellers, D_{coax_1} and D_{coax_2} are drag moments of the coaxial fan propellers, l_1 and l_2 are moment arms, ζ is an angle between l_1 and body Y axis. In [1], a detailed description of motor-propeller configuration and performance test results are given.

In hover regime, there is no aerodynamic force and moment acting on the UAV body because of the absence of the forward airspeed. When the front motors start to rotate about the tilting axis, horizontal force is created proportional to the tilting angle. So, aerodynamic lift force, drag force, and pitching moment affect the airframe, as shown in Fig. 5.

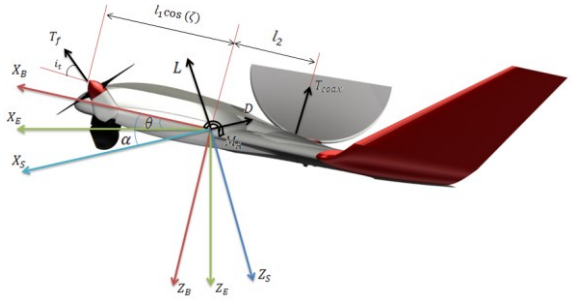

Figure 5. Forces and moments on the TURAC in transitional flight.

If it is assumed that the wing level of the UAV is controlled with a control system, lateral dynamics can be ignored and equations of motion of longitudinal transitional flight are formed as shown in (8-9).

$$\begin{aligned} &\mathrm{m}(\dot{\mathrm{U}} + \mathrm{QW} - \mathrm{RV}) \\ &= -\mathrm{mg\,s\theta} + (-\mathrm{D\,c\alpha} + \mathrm{L\,s\alpha}) + \mathrm{T_f\,ci_t} \\ &\mathrm{m}(\dot{\mathrm{W}} + \mathrm{PV} - \mathrm{QU}) \\ &= \mathrm{mg\,c\phi\,c\,\theta} + (-\mathrm{D\,s\alpha} - \mathrm{L\,c\alpha}) + (-\mathrm{T_f\,si_t} - \mathrm{T_{coax}}) \\ &\dot{\mathrm{Q}}\mathrm{I_{yy}} - \mathrm{PR}(\mathrm{I_{zz}} - \mathrm{I_{xx}}) + (\mathrm{P^2} - \mathrm{R^2})\mathrm{I_{xz}} \\ &= \mathrm{M_A} + (\mathrm{T_f l_1\,si_t\,c\zeta} - \mathrm{T_{coax} l_2}) \end{aligned} \tag{8}$$

Coordinate equations

$$\begin{aligned} &\dot{x}_E \\ &= U\,c\theta\,c\psi + V(s\phi\,s\theta\,c\psi - c\phi\,s\psi) \\ &+ W(c\phi\,s\theta\,c\psi + s\phi\,s\psi) \end{aligned} \tag{9}$$

$$\dot{z}_E = -U\,s\theta + V\,s\phi\,c\theta + W\,c\phi\,c\theta$$

In Eq. (8-9), "s" and "c" are used for sine and cosine functions.

Figure 6: Airflow vectors acting on the UAV.

Aerodynamic forces and moments exerted on the UAV are functions of total airflow vector, V_T. Hence, it is important to determine the magnitude and direction of the total airflow. As shown in Fig. 6, there are two airflow vectors acting on the UAV. The first one is V_∞ and it is generated by translational motion. The components of V_∞ are body axis velocity vectors U and W. The second airflow vector acting on the body is propeller-induced airflow V_{out}. It is a function of front propeller thrust T_f, air density ρ, propeller area A and intake airflow velocity of the propeller V_{in}.

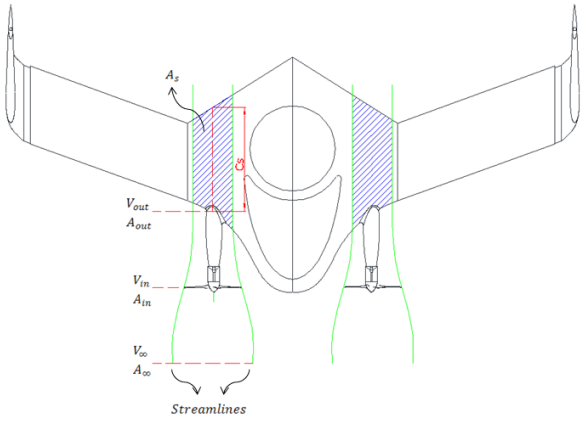

Figure 7: Propeller induced airflow effects on the UAV body.

Input and output velocities of the propeller are shown in Fig. 7. They are calculated using classical momentum theory as shown in (10) and (11).

$$V_{in} = \frac{V_\infty c\alpha\, ci_t + V_{out}}{2} \tag{10}$$

$$V_{out} = \sqrt{\frac{2T_f}{\rho\pi R_p^2} + (V_\infty c\alpha\, ci_t)^2} \tag{11}$$

According to the continuity equation, output cross section area of the propeller induced airflow changes as a function of V_{in} and V_{out} as shown in (12).

$$A_{out} = \frac{\pi R_p^2 V_{in}}{V_{out}} \tag{12}$$

In transitional and horizontal flight, the total airflow vector flows over in a specific area (A_s) on the UAV body as shown in Fig (7) and it is calculated geometrically as shown in (13).

$$A_s = 2R_s c_s \tag{13}$$

where c_s is mean aerodynamic chord of the specified region as shown in Fig. (7).

In hover flight, the thrust axis of the tilt rotors is perpendicular to the body X axis. So, any propeller induced effects are not observed on the body. However, when the tilt angle starts to decrease, additional forces and moments are generated due to the propeller airstream. Effectiveness of the propeller induced airspeed on the UAV body is modeled as a sigmoid function $\xi \in [1, 0]$ as shown in (14) and Fig. (8).

$$\xi = 1 - \frac{1}{1 + e^{-0.15(i_t - 45)}} \tag{14}$$

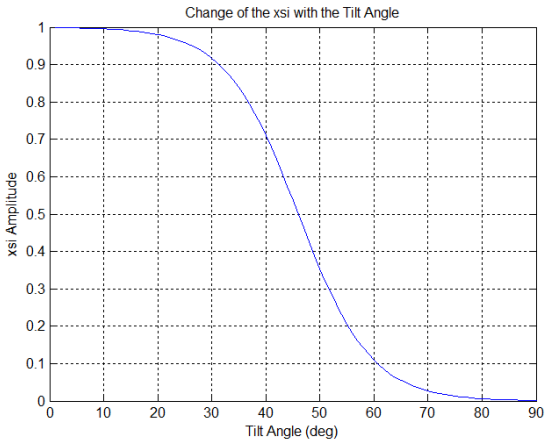

Figure 8: Change of effectiveness coefficient with the tilt angle.

The effectiveness coefficient ξ is used to calculate the total effective velocity on the body profile while the tilt angle value is between 0 and 90 degrees. Hence, the total airspeed that acting on the above-mentioned area A_s is defined as shown in (15).

$$V_T = \sqrt{(V_{out}\,\xi\,\sin(\alpha + i_t))^2 + (V_{out}\,\xi\,\cos(\alpha + i_t) + V_\infty)^2} \tag{15}$$

Both the free airstream and the propeller-induced airstream are effective on A_s. Therefore, the total airspeed (V_T) is used to calculate the lift force, drag force and pitching moment generated on A_s as shown in (16).

$$\begin{aligned} L_s &= \frac{1}{2}\rho V_T^2 A_s C_{L_s} \\ D_s &= \frac{1}{2}\rho V_T^2 A_s C_{D_s} \\ M_s &= \frac{1}{2}\rho V_T^2 A_s c_s C_{M_s} \end{aligned} \tag{16}$$

Aerodynamic coefficients in (16) are obtained as shown in (17) and aerodynamic derivatives are calculated using 2D analysis of the body airfoil.

$$\begin{aligned} C_{L_s} &= C_{L_{s_0}} + C_{L_{s_{\alpha_{eff}}}}\alpha_{eff} + C_{L_{s_{\delta_e}}}\delta_e \\ C_{D_s} &= C_{D_{s_0}} + C_{D_{s_{\alpha_{eff}}}}\alpha_{eff} + C_{D_{s_{\delta_e}}}\delta_e \\ C_{M_s} &= C_{M_{s_0}} + C_{M_{s_{\alpha_{eff}}}}\alpha_{eff} + C_{M_{s_{\delta_e}}}\delta_e \end{aligned} \tag{17}$$

where α_{eff} is the effective angle of attack on the wing which is produced by propeller-induced airstream and free airstream. α_{eff} is calculated using (18).

$$a_{eff} = a + a_s = arctan\left(\frac{V_2 sin(a + i_T)}{V_2 cos(a + i_T)}\right) \tag{18}$$

On the remaining region $(A - A_s)$, aerodynamic forces and pitching moment are generated by the free airstream. So, the forces and pitching moment are calculated as shown in (19).

$$\begin{aligned} L_w &= \frac{1}{2}\rho V_\infty^2 (A - A_s) C_{L_w} \\ D_w &= \frac{1}{2}\rho V_\infty^2 (A - A_s) C_{D_w} \\ M_w &= \frac{1}{2}\rho V_\infty^2 (A - A_s) c C_{M_w} \end{aligned} \tag{19}$$

where A is the planform area of the UAV. Aerodynamic coefficients in (19) are obtained as shown in (20) and aerodynamic derivatives are calculated using 3D analysis of the whole airframe.

$$\begin{aligned} C_{L_w} &= C_{L_{w_0}} + C_{L_{w_\alpha}}\alpha + C_{L_{w_{\delta_e}}}\delta_e \\ C_{D_w} &= C_{D_{w_0}} + C_{D_{w_\alpha}}\alpha + C_{D_{w_{\delta_e}}}\delta_e \\ C_{M_w} &= C_{M_{w_0}} + C_{M_{w_\alpha}}\alpha + C_{M_{w_{\delta_e}}}\delta_e \end{aligned} \tag{20}$$

Propeller intake airflow speed (V_{in}) is an important factor on the generated thrust. The angle of attack on the propeller blades decreases as intake airflow speed increases. So, thrust decreases because of the low angle of attack on the blades. In Fig. (9), propeller intake airflow speed—generated thrust characteristics of the 26x13-inch fixed-pitch propeller are shown for various RPM During transitional flight, front propellers turn at about 5000 rpm. Maximum thrust is generated at near-hover flight conditions because of the low intake airflow speed. As the tilt angle decreases, propeller intake airflow speed increases and generated thrust decreases. In near-hover flight, each propeller produces about 13 kg of thrust force. However, at a cruise speed of 20 m/s, propellers produce about 5 kg of thrust force because of the above-mentioned aerodynamic effect. This thrust–airspeed relationship is modeled using the curve-fitting technique for 5000 rpm and a cubic function is obtained, as shown in (21). This function is integrated into the nonlinear mathematical model of transitional flight.

$$f_T(V_{in}) = -0.00036027\,{V_{in}}^3 + 0.023793\,{V_{in}}^2 - 0.7321\,V_{in} + 12.932 \quad (21)$$

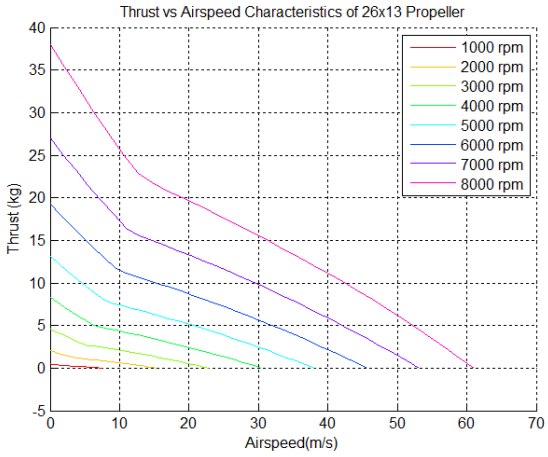

Figure 9: Thrust - propeller intake airflow speed characteristics of the 26x13 fixed-pitch propeller.

Nonlinear transitional-flight EOMs were constructed in Matlab/Simulink, as shown in Fig. 10. Control inputs were sent with helicopter-simulator hardware that includes cyclic and collective. Also, a soft real-time block was used to synchronize the model clock and the real clock.

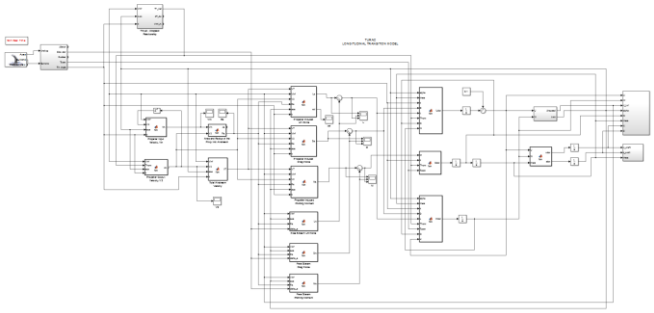

Figure 10: Block diagram of the real time nonlinear transition model.

After the construction of the nonlinear mathematical model of transitional flight, simulation studies were performed with a pilot in the real-time simulator. In Fig. 11, flight path of the transitional flight is shown.

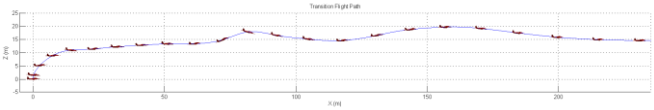

Figure 11: Transition flight path.

Figure 11: Transitional flight path.

The position of the UAV accoring to the Earth axis (X, Z), body axis velocities (U, V), and pilot's control inputs are shown in Fig. 12, Fig. 13, and Fig. 14.

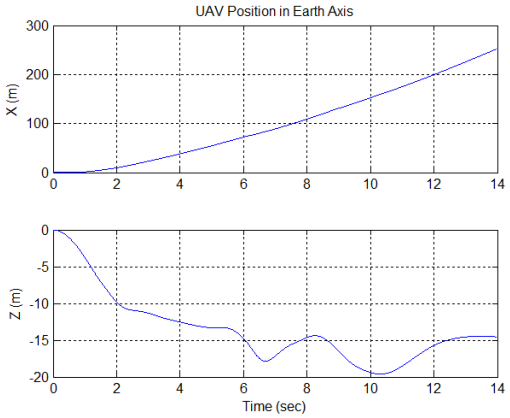

Figure 12: UAV position in Earth axis.

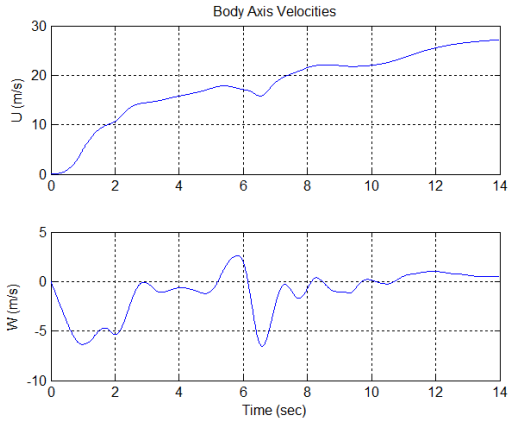

Figure 13: Body axis velocities of the UAV.

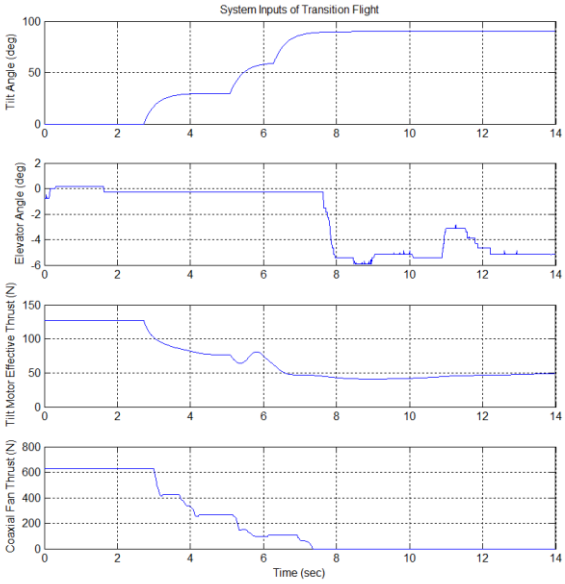

Figure 14: Pilot's control inputs in transition flight regime.

Transition Scenario

Total force in x and z directions and moment around aerodynamic center are calculated using (22). Positive direction is lift direction at $\sum F_z$ and thrust direction at $\sum F_x$ [22].

$$\begin{aligned} F_z &= L_w + 2T(sini_T)(cosa) + L_s cos(a_w) - D_s sin(a_w) \\ &+ T_{coax} cosa - W \\ F_x &= 2T(cosi_T)(cosa) - D_w - L_s sin(a_w) - D_s cos(a_w) \\ &- T_{coax} sina \\ M_{ac} &= 2T sini_T(x_{AC} - x_T) + T_{coax}(x_{AC} - x_{T_{coax}}) \\ &+ W(x_{AC} - x_W) cosa \end{aligned} \quad (22)$$

Also, pitching moment coefficient is obtained using (23).

$$C_M = \frac{M_{ac}}{\frac{1}{2}\rho V^2 cS} + C_{M_{\delta_e}}\delta_e \quad (23)$$

Various scenarios are calculated by utilizing the above equations. In the first scenario, tilt angle increases with increase in airspeed. In the second scenario, tilt angle and positive angle of attack are constant. In the third scenario, tilt angle and negative angle of attack are constant. The force and moment value of the third scenario has the best results. Tilt angle is set at 70° and angle of attack at -1° until 20 m/s. Above this velocity, tilt angle decreases to 0° and the angle of attack is around 2°. In Table 2, the force and moment coefficient values are given for the third scenario.

Table 2. The force and moment coefficient for the third scenario.

.

V	i_T (°)	α (°)	T_f (N)	T_{coax} (N)	$\sum F_x$	$\sum F_z$	C_M
2	70	-1	73.2	329.6	48.6	0.071	-0.0004
5	70	-1	72.6	326.7	46.2	0.003	-0.005
10	70	-1	70.4	317.7	39.3	0.001	-0.0056
15	70	-1	70.7	296	30.5	0.002	0
20	70	-1	66	172	14	-0.007	0.0076
22	0	2.25	75.7	0	114	0.009	0.0009
22	0	2.5	36	0	34.7	0.0062	0.0009
24	0	2	19.6	0	0	0.073	-0.0054

In the scenario with 20 m/s airspeed elevator angle (δ_e) is 10° and at 22 m/s airspeed it is -3°. In this scenario, excess thrust occurs at each velocity. Moment coefficient and $\sum F_z$ equals zero, so the UAV is at balance and accelerates. At 24 m/s, the balance of UAV occurs and all forces and moment coefficients are zero at -2.28° elevator angle. By using these calculations different types of scenarios can be developed.

III. CFD Analysis

In this study, aerodynamic coefficients of TURAC in transition-flight regime are defined using the CFD method. It includes four steps: creating control volume, meshing, building boundary layer, and analyzing set up. Fluent is used to solve the equations.

CFD analyses have been done up to 75° tilt angle with 0° angle of attack. In CFD analyses, one of the vital issues is the value of y^+ which should be between 1 and to reach accurate results in the viscous region. For high quality analysis, it is taken as 1. Additionally, the first height of the boundary layer for transitional flight is defined according to Reynold's number and the y^+ value. The K-epsilon Realizable Enhanced Wall Treatment turbulent model is obtained for the CFD case. The transition-flight analysis is also explained as, "Low cost prototyping, analyzing, and flight testing for the TURAC VTOL UAV" study [1].

For higher tilt angles, CFD models were created and analyses are performed. However, results did not converge. According to this problem, force and moment mathematical equations were developed for the transitional flight regime. Various scenarios were created with respect to different tilt angles and angles of attack during transition.

In the transitional flight regime, tilt rotors and the coaxial rotor operate. At the beginning of transitional flight, tilt rotor axis of rotation is perpendicular to the body axis. During the transition, front propellers are tilted until their axis is in the same direction as body axis. In this regime, flowfield around TURAC and rotor/wing interaction is extremely complex.

Models

In the transitional flight regime, TURAC is modeled with an open-fan concept. In the model, TURAC and four rotors are modeled and meshed. Two rotors are positioned for coaxial main lift fan and another two rotors for tilt rotors. All rotors are modeled as actuator discs; tilt angle (i_t) is 90° in hover position and 0° in forward flight position. In Fig. 15, the UAV is modeled for 75° tilt angle and 0° angle of attack.

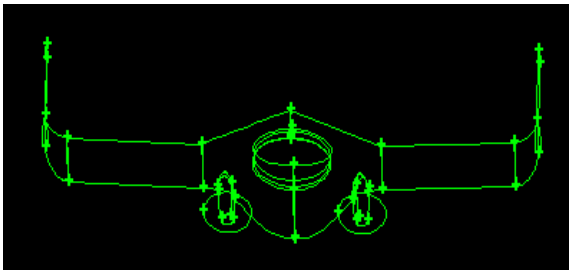

Figure 15. TURAC model for the transitional flight regime at i_t=75°.

The first cell height for the boundary layer is calculated with Reynold's number and the y^+ value.

Analysis

The aerodynamic analysis of TURAC in transitional flight was done with Fluent. In this regime, a turbulence model is selected, the k-epsilon Realizable Enhanced Wall Treatment and Green-Gauss Node Based solver are utilized. In the analysis, rotors are defined as fan-boundary conditions. Inlet is defined as velocity inlet and outlet is determined as pressure outlet. At fan-boundary condition surfaces, the pressure difference between forward and aft of the rotor which is called pressure jump, calculated with the thrust of the rotor. Pressure jump is inserted to the analyze set up for each rotor. TURAC is analyzed at a 75° tilt angle with 0° angle of attack in different forward velocities. Results are presented as C_L-V, L-V, C_D-V and D-V graphs in the figures below.

The velocity contour of TURAC can be seen in Fig. 34. The rotors of the coaxial main lifting fan are shown in the figure below. The velocity contour is at the symmetry plane of the UAV due to fuselage axis. In cases with higher freestream velocity, the flow below the coaxial fan moves backward in the same direction as the freestream velocity. In Fig. 16, increased velocity behind the coaxial fan can be seen clearly.

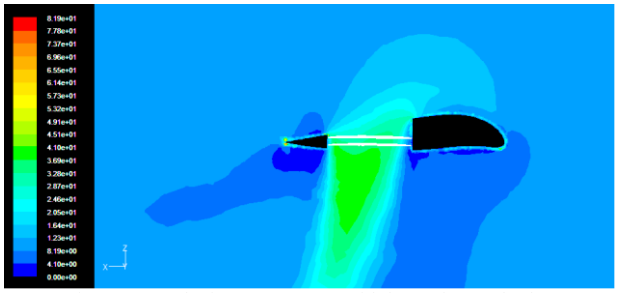

Figure 16. Velocity contours on midplane of UAV body.

In Fig. 17, the streamlines follow the upper surface of the body and enter the open fan. According to this, the elevator effect on TURAC reduces dramatically during transitional flight. The vortices behind UAV increase because of the tilt and coaxial rotors.

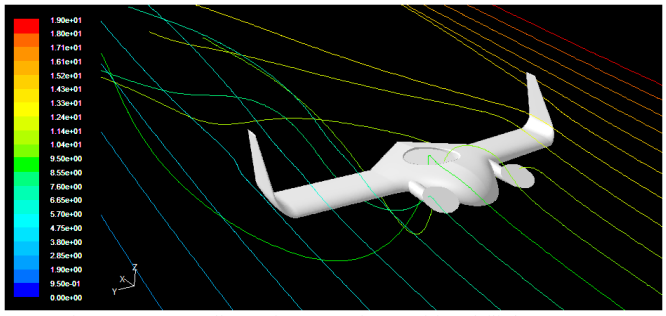

Figure 17. Streamlines of TURAC in transitional flight i_t=75°.

Transitional flight analysis of TURAC at i_t=75° was done at 20, 10, 9.5 and 5 m/s with 0° angle of attack. The reason for analyzing TURAC at 9.5 m/s is to understand whether the drag force changes linearly. If it changes linearly between 5 and 10 m/s, it should be zero at 9.5 m/s. As a result, the 9.5 m/s test shows the change of force is not linear with respect to velocity.

Lift coefficient versus velocity in transitional flight can be seen in Fig. 18. Lift coefficient increases up to 9.5 m/s forward speed at the same angle of attack. Then, it decreases until 20 m/s. To show this clearly, lift force is plotted in Fig. 19. Lift force does not change linearly from 5–20 m/s forward velocity. At first glance, lift coefficient around 10 m/s seems high, but the lift force is produced by the airframe of UAV, the z component of coaxial fan, and the tilt rotors' thrust. In the transitional flight regime analyses, each tilt rotor was set 70 N thrust and the coaxial fan to 350 N thrust. The lift coefficient in the figure below is normally higher than regular values due to the thrust.

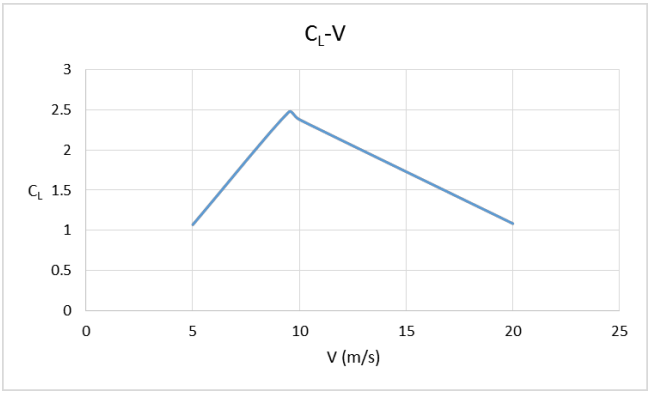

Figure 18. Lift coefficient vs TURAC velocity at i_t=75° and α=0°.

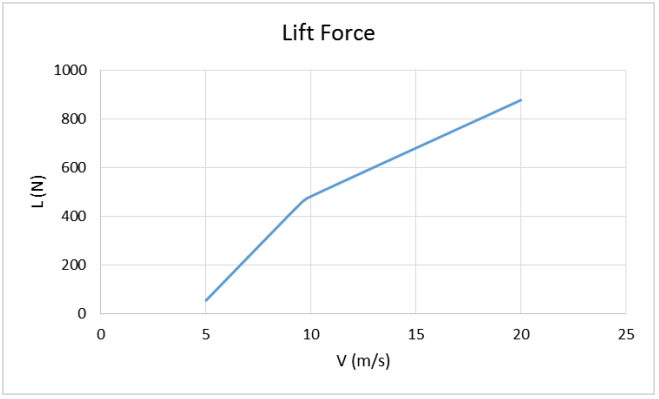

Figure 19Lift force vs. TURAC velocity at i_t=75° and α=0°.

Drag force and coefficient versus velocity is presented in Fig. 20-21. The drag force direction is assumed to be positive in the x direction. The drag force and coefficent are negative below 10 m/s because tilt-rotor thrust is higher than drag force. So the vector difference between these forces is also in the thrust force direction. In Fig. 20, the UAV drag coefficent seems constant at velocities higher than 10 m/s. Drag force increases as velocity increases. As shown to Fig. 21, drag force equals tilt-rotor thrust between 5 and 10 m/s.

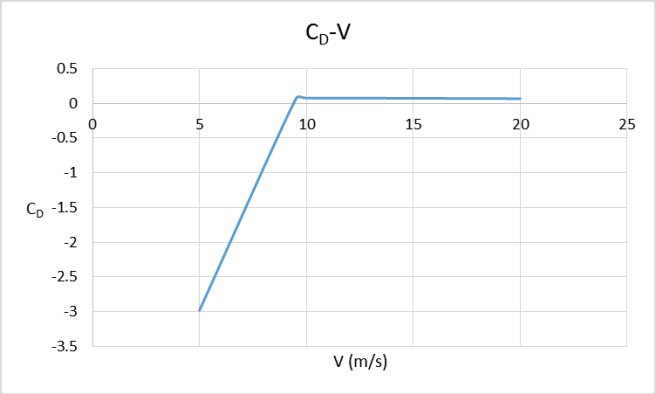

Figure 20. Drag coefficient vs. TURAC velocity at at i_t=75° and α=0°.

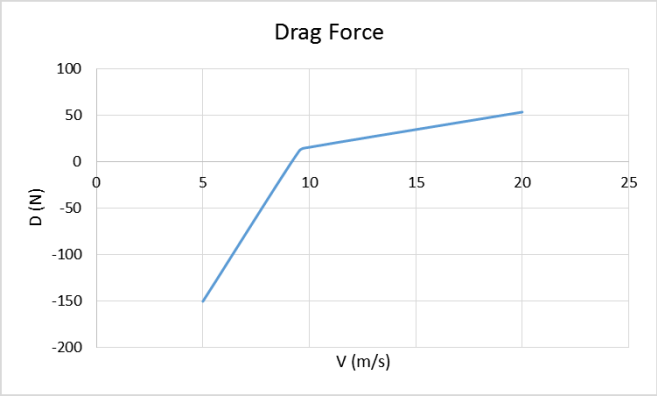

Figure 21. Lift force vs. TURAC velocity at i_t=75° and α=0°.

At higher tilt angles, CFD analysis were done, however results did not converge. Therefore, force and moment equations were developed with propeller effect. Some scenarios were investigated with different tilt angles and angles of attack. The calculations and results are explained elaborately in the following section.

IV. CONCLUSION

Nonlinear mathematical models of the TURAC civil tilt-rotor VTOL UAV were obtained for the transition-flight regime. Longitudinal EOMs of transitional flight were derived based on Newton's second law. Aerodynamic effects of the free airstream and propeller induced airstream on the UAV were modeled individually. A transition simulator was structured using the above-mentioned EOMs and real-time simulation was performed.

Transition-flight regime analyses were evaluated at different velocities with 0° and 15° angles of attack. Lift and drag forces increased with angle of attack. Given convergence problems at higher tilt angles, aerodynamic analysis was done with mathematical equations. Force and moment equations including propeller effect produced satisfactory results. At 70° tilt angle and -1° angle of attack, velocity increased. Balance points, $\sum F_z$ and C_M at zero, are defined. At the balance points, excess thrust was observed, which means UAV accelerates. The force and moment values from the equations are accurate for transitional flight.

REFERENCES

[1] Y. O. Aktas, U. Ozdemir, Y. Dereli, A. F. Tarhan, A. Cetin, A. Vuruskan, B. Yuksek, H. Cengiz, S. Basdemir, M. Ucar, M. Genctav, A. Yukselen, I. Ozkol, M. O. Kaya, G. Inalhan, "A low cost prototyping, analyzing and flight testing for the TURAC VTOL UAV", Submitted for Review for Publication ICUAS 2014, Orlando, May 27-30, 2014.

[2] S. Bouabdallah, P. Murrieri, R. Siegwart, "Design and control of an indoor micro quadrotor", *International Conference on Robotics and Automation,* New Orleans, LA, April 2004

[3] S. Bouabdallah, "Design and control of quadrotors with application to autonomous flying", PhD thesis, Ecole Polytechnique Federale de Lausanne (EPFL), Thesis No: 3727, February 23, 2007.

[4] A. Okan, O. Tekinalp, M. S. Kavsaoğlu, O. Armutcuoglu, E. Tulunay, "Flight mechanics analysis of a tilt-rotor UAV", *AIAA Paper-99-4255.*

[5] G. R. Flores, J. Escareno, R. Lozano, S. Salazar, "Quad-tilting rotor convertible mav: modeling and real-time hover flight control", *Journal of Intelligent and Robotic Systems*, vol. 65, 2012, pp. 457-471.

[6] G. Flores, R. Lozano, "Transition flight control of the quad-tilting rotor convertible MAV", *2013 International Conference on Unmanned Aircraft Systems (ICUAS)*, Atlanta, May 28-31, 2013.

[7] V. Gupta," Quad tilt rotor simulations in helicopter mode using computational fluid dynamics", PhD thesis, University of Maryland, 2005.

[8] M. A. Postdam, R. C. Strawn, "CFD simulations of tiltrotor configurations in hover", at the American Helicopter Society 58th Annual Forum, June 11-13, 2002.

[9] L. A. Young, D. Lillie, M. McCluer, G. K. Yamauchi, "Insights into airframe aerodynamics and rotor-on-wing interactions from a 0.25-scale tiltrotor wind tunnel model", *AHS International Aerodynamics, Acoustics, and Test and Evaluation Specialists' Conference,* San Francisco, CA, January 23-25, 2002.

[10] C. Matos, U. Reddy, N. Komerath, "Rotor wake/fixed wing interactions with flap deflection", *American Helicopter Society 55th Annual Forum,* Montreal, Canada, May 25-27, 1999.

[11] C. A. M. Matos, "Download reduction on a wing-rotor configuration", PhD thesis, Georgia Institute of Technology, December 2001.

[12] H. Yeo, W. Johnson, "Performance and design investigation of heavy lift tilt-rotor with aerodynamic interference effects", *Journal of Aircraft,* vol. 46, No. 4, July–August 2009, pp. 1231-1239.

[13] R. M. Cummings, S. A. Morton, S. G. Siegel, "Numerical prediction and wind tunnel experiment for a pitching unmanned combat air vehicle", *Aerospace Science and Technology,* vol. 12, 2008, pp. 355-364.

[14] W. Wisnoe, R. E. M. Nasir, W. Kuntjoro, A. Mohd, I. Mamat, "Wind tunnel experiments and CFD analysis of Blended Wing Body (BWB) Unmanned Aerial Vehicle (UAV) at mach 0.1 and mach 0.3", *13th International conference on Aerospace Sciences & Aviation Technology,* ASAT- 13, May 26 – 28, 2009.

[15] M. Lino, "Numerical investigation of propeller-wing interaction effects for a large military transport aircraft", PhD thesis, Delft University of Technology, August 27, 2010.

[16] C. Kim, J. Chung, "Aerodynamic analysis of tilt-rotor unmanned aerial vehicle with computational fluid dynamics, *Journal of Mechanical Science and Technology,* Vol. 20, No.4, pp. 561-568, 2006.

[17] J. Abbas, R. Narducci, "Analysis of CFD modeling techniques over the mv-22 tiltrotor", *American Helicopter Society 66th Annual Forum*, Phoenix, AZ, May 11-13, 2010.

[18] B. Sweeten, "CFD analysis of UAVs using Vorstab, Fluent, and Advanced Aircraft Analysis software", Master Thesis, University of Kansas, April 27, 2010.

[19] R. C. Nelson, *Flight Stability and Automatic Control,* 2nd ed., Singapore, McGraw-Hill, 1998, ch.3-5.

[20] J. H. Blakelock, *Automatic Control of Aircraft and Missiles,* 2nd ed., USA: John Wiley & Sons, 1991, ch. 1,3.

[21] T. R. Yechout,, *Introduction to Aircraft Flight Mechanics,* VA: AIAA Education Series, 2003, ch. 4-6.

[22] Advisory Group for Aerospace Research and Development (AGARD), "The Aerodynamics of V/STOL Aircraft", AGARDograph 126, May 1968.